Eur Biophys J (1997) 26: 307–318

ARTICLE

K. Tönsing · S. Kakorin · E. Neumann
S. Liemann · R. Huber

Annexin V and vesicle membrane electroporation

Received: 9 January 1997 / Accepted: 21 April 1997

Abstract The method of membrane electroporation (ME) has been used as an analytical tool to quantify the effect of membrane curvature on transient electric pore formation, and on the adsorption of the protein annexin V ($M_r = 35{,}800$) to the outer surface of unilamellar lipid vesicles (of radii $25 \le a/nm \le 200$). Relaxation kinetic studies using optical membrane probes of the diphenylhexatriene type suggest that electric pore formation is induced by ionic interfacial polarization causing entrance of the (more polarizable) water into the lipid bilayer membrane yielding (hydrophobic and hydrophilic) pore states with a mean stationary pore radius $r_p = 0.35$ (±0.05) nm. Extent and rate of ME, compared at the same induced transmembrane voltage, were found to decrease both with increasing vesicle radius and with increasing protein concentration. This 'inhibitory' effect of annexin V is apparently allosteric and saturates at about $[AN_T]_{sat} = 4$ μM annexin V for vesicles of $a = 100$ nm at 1 mM total lipid concentration, 0.13 mM total Ca^{2+} concentration and at $T = 293$ K. Data analysis in terms of Gibbs area-difference-elasticity energy suggests that the bound annexin V reduces the gradient of the lateral pressure across the membrane. At $[AN_T]_{sat}$, about 20% of the vesicle surface is covered by the bound protein, but it is only 0.01% of the surface of the outer lipid leaflet in which a part of the protein, perhaps the aromatic residue of the tryptophan (W 187), is inserted. Insertion leads to a denser packing of the lipid molecules in the outer membrane leaflet. As a consequence, the radius of the electropores in the remaining membrane part, not covered by annexin V decreases ($r_p/nm = 0.37$, 0.36 and 0.27) with increasing adsorption of the protein ($[AN_T] = 0$, 2 and 4 μM, respectively).

Key words Annexin V · Lipid vesicles · Electroporation · Diphenylhexatriene-labeled phospholipids (β-DPH pPC) · Absorbance dichroism

Abbreviations PA phosphatidic acid · PE phosphatidylethanolamine · PS phosphatidylserine · POPC palmitoyloleoylphosphatidylcholine · Trp tryptophan · β-DPH pPC 2-(3-(diphenylhexatrienyl)propanoyl)-1-hexadecanoyl-sn-glycero-3-phosphocholine · $[AN_T]$ total and [AN] free annexin V concentrations, respectively · C closed lipid bilayer state · HO hydrophobic pore state · HI hydrophilic pore state · (L_n) cluster of n lipids (L) · a vesicle radius · ME membrane electroporation

I Introduction

The human placental anticoagulant protein, annexin V ($M_r = 35{,}800$), is a member of the annexin family of structurally homologous proteins interacting with anionic phospholipid membranes in a calcium dependent manner (for a review, see Raynal and Pollard 1994; Swairjo and Seaton 1994). The apparent dissociation equilibrium constant for the binding of Ca^{2+} to annexin V, in the absence of acidic lipids, is $K_{Ca} \approx 10^{-4}$ M. In the presence of 10 to 100 μM Ca^{2+}, annexin V binds to acidic lipids such as PS, PE, PA with high affinity, $K_{AN} \approx 10^{-10}$ M at physiological ionic strength (Schlaepfer et al. 1987; Tait et al. 1989; Tait and Gibson 1992). The structure of annexin V has been solved, both in the water soluble form by high resolution X-ray crystallography (Huber et al. 1990a, b; 1992) as well as in the lipid monolayer bound form by medium resolution electron image analysis of two-dimensional crystals (Mosser et al. 1991; Brisson and Mosser 1991; Voges et al. 1994). The comparison of these structures specifies the orientation of the molecule with respect to the membrane.

K. Tönsing · S. Kakorin · E. Neumann (✉)
Physical and Biophysical Chemistry, Faculty of Chemistry, University of Bielefeld, P.O. Box 100 131, D-33501 Bielefeld, Germany
(Fax: 49-5 21-1 06 29 81;
e-mail: eberhard.neumann@post.uni-bielefeld.de)

S. Liemann · R. Huber
Max-Planck-Institut für Biochemie, Am Klopferspitz 18a, D-82152 Martinsried, Germany

The binding of annexin V to lipid monolayers apparently causes no major structural changes compared with the crystal structure. The crystal structure analysis revealed a central hydrophilic pore through the molecule, containing buried charged residues and water molecules. The pore is suggested to be an ion conduction pathway (Huber et al. 1992; Demange et al. 1994). Patch-clamp measurements show that annexin V exhibits typical ion channel features (Voges et al. 1995; Liemann et al. 1996) such as voltage-gating and ion selectivity.

Annexin V contains a single tryptophan (Trp 187) in the consensus sequence region of the third 70-amino acid repeat (Huber et al. 1992). Ca^{2+} binding to annexin V results in a conformational change that exposes Trp 187 in a position where it can make contact with membrane phospholipids (Meers and Mealy 1994). The large change in the tryptophan fluorescence caused by annexin V binding to the phospholipid bilayer can be used to monitor the Ca^{2+} dependent binding process (Meers 1990; Meers and Mealy 1993a, b; 1994). Besides fluorescence spectroscopy, the binding of annexin V to vesicular lipid bilayers has been studied by various methods such as electron microscopy (Voges et al. 1994), neutron scattering techniques (Ravanat et al. 1992) and ^{31}P- and ^{1}H-nuclear magnetic resonance (NMR) (Swairjo et al. 1994).

Here, we use the method of membrane electroporation (Neumann et al. 1982, 1992; Kakorin et al. 1996) to investigate the Ca^{2+} dependent interaction of annexin V with lipid bilayers of vesicles of different diameters. The electroporation technique has been applied so far to manipulate biological cells and organelles, cell aggregates and tissue; the various cell biological applications include the direct (electrophoretic) transfer of genes (Neumann et al. 1982, 1996), of proteins, dyes and drugs into the cell interior and recently, the electroporative chemotherapy of skin cancers (e.g., Heller et al. 1996). The molecular mechanism of electroporation has been derived from electro-optic relaxation data and formulated in terms of a specific chemical model for the electric pore formation due to local water entrance and structural changes of the bilayer (Kakorin et al. 1996). Here, we found that bound annexin V reduces the electroporation sensitivity of the lipid bilayer, probably by decreasing the local membrane curvature.

II Materials and methods

Materials

Synthetic POPC from Avanti Polar Lipids, Inc. (Birmingham, AL 35007, U.S.A.) and bovine brain extract type III (containing 80–85% PS) from Sigma Chemie GmbH (Deisenhofen, Germany) were used without further purification. The optical lipid probe 2-(3-(diphenylhexatrienyl)propanoyl)-1-hexadecanoyl-sn-glycero-3-phosphocholine (β-DPH pPC, $M_r = 782$) was from Molecular Probes, Inc. (OR, U.S.A.). All other chemicals were of the purest available grade.

Annexin V preparation

Recombinant annexin V wild-type protein was expressed and purified as previously described (Burger et al. 1993). The protein was quantified by the absorbance A_{280} at the wavelength $\lambda = 280$ nm, assuming $A_{280} = 6$ at a concentration of 10 mg/mL or 279 μM (Funakoshi et al. 1987) yielding the absorbance coefficient $\varepsilon_{280} = 21{,}508\ M^{-1}\ cm^{-1}$ at $T = 293$ K (20 °C). Determination of the protein concentration with the bicinchoninic acid (BCA) reagent (Pierce Europe b.v, Holland) according to the manufacture's instructions (Smith et al. 1985) yielded the same results as the A_{280}-measurements (data not shown).

Vesicle preparation

Large unilamellar phospholipid vesicles (LUV) and β-DPH pPC doped vesicles (DPH-LUV) were prepared by the extrusion method (Mayer et al. 1986). Phospholipids and β-DPH pPC dissolved in ethanol were mixed in the molar ratio of 200 : 1 in chloroform and dried under vacuum, using a rotary evaporator. At the ratio 200 : 1, the concentration of the optical probe was [β-DPH pPC] = 5 μM. The dry lipid film thus obtained was maintained under vacuum for at least 30 min to remove any residual solvent. The lipid was resuspended in 0.66 mM HEPES-Na-buffer, pH 7.4, at the total concentration $[CaCl_2] = 0.13$ mM, where annexin V is completely bound, to a final concentration of 10 mg phospholipid/mL solution. The buffer was filtered through a 0.2 μm filter prior to use. The lipid suspension was frozen and thawed five times using liquid nitrogen and a warm water bath, followed by 21 passes through polycarbonate membrane filters (Avestin/Milsch, Germany), respectively, using a LiposoFast-Basic extruder (Avestin/Milsch, Germany). The vesicle mean diameters were determined by dynamic light scattering measurements (data not presented) and were ∅/nm = 70 (±18), 100 (±36), 180 (±55) and 300 (±91) after extrusion through the 50-, 100-, 200- and 400-nm filters, respectively; in line with the size distribution of extruded vesicles determined by Mayer et al. (1986). During the vesicle preparation and the following electro-optic relaxation measurements care was taken to protect the DPH-samples from light photolysis.

The final total lipid concentration used for the optical (fluorescence, OD) and electro-optical measurements was $[L_T] = 1$ mM, corresponding to a vesicle density of $\approx 7.6 \cdot 10^{14}$/L for vesicles of radius $a = 150$ nm. Under these conditions, the average distance between the surfaces of single vesicles is $x \approx 1.1$ μm, qualifying the suspension as diluted (practically no vesicle-vesicle contacts at low [Ca]). In an electric field ($E = 8$ MV/m) the minimum characteristic time t_{app} of approach of vesicles ($a = 150$ nm) due to induced dipole forces (Foster and Sowers 1995) was calculated by taking into account the hydrodynamic interactions (Batchelor 1976). If the term $u = (\varepsilon_{eff} - \varepsilon_w)/(\varepsilon_{eff} + 2\varepsilon_w)$ of Foster and Sowers is applied to the vesicle bilayer shell, ε_{eff} is the effective relative permittivity of the

electroporated bilayer and $\varepsilon_w = 80$ is that of water. Since in any case $\varepsilon_{eff} \ll \varepsilon_w$ and probably $\varepsilon_{eff} \geq \varepsilon_L$, where $\varepsilon_L = 2.1$ (lipid), here $|u| \leq 0.5$ and the minimum time is $t_{app} \geq 56$ µs. At a pulse duration of $t_E = 10$ µs and at field strengths $E \leq 8$ MV/m and for vesicle radii $a \leq 150$ nm, we may therefore safely neglect vesicle-vesicle interactions.

Fluorescence measurements and binding assay

The extent of annexin V binding to phospholipid vesicles was monitored by tryptophan fluorescence emission in the presence of 0.13 mM total Ca^{2+} concentration at $T = 293$ K (20 °C). The vesicles were mixed with the indicated amount of annexin V in a quartz cuvette. After incubation for 15 min, fluorescence intensity was recorded on a Hitachi fluorescence spectrophotometer F-4010. The excitation wavelength was $\lambda_{ex} = 295$ (±1) nm, where the sole tryptophan residue (Trp 187) is selectively excited. Emission was recorded at a single wavelength $\lambda_{em} = 338$ (±2) nm or by scanning from 300 to 400 (±2) nm. Buffer blanks (see Section Vesicle preparation) were subtracted under the same experimental conditions.

OD measurements

OD measurements were used to monitor the binding of annexin V to phospholipid vesicles and to determine the absorbance spectrum $A(\lambda)$ of the optical membrane reporter lipid β-DPH pPC. OD spectra were recorded with a Uvikon 943 Double Beam UV/VIS Spectrophotometer (Kontron Instruments) between 300–500 nm, using quartz cuvettes with 1 cm optical path length.

Electro-optical relaxation measurements

Electro-optic relaxation spectrometry was used to record the field induced changes in the optical properties of lipid systems in solution. Rectangular pulses of field strength up to 8 MV m^{-1} and of duration up to $t_E = 10$ µs can be applied by cable discharge to the sample cell equipped with parallel planar graphite electrodes, which was thermostated at $T = 293.0$ (±0.1) K (20 °C). The field induced changes in the transmittance of plane-polarized light was measured at the wavelength $\lambda = 365$ nm (Hg-line; highest accuracy).

The light intensity change ΔI^σ, caused by the electric pulse and measured at the polarization angle σ relative to the direction of the applied external field vector E, is related to the optical density change ΔOD^σ by

$$\Delta OD^\sigma = OD^\sigma(E) - OD_0^\sigma = -\log(1 + \Delta I^\sigma / I^\sigma) \quad (1)$$

where $\Delta I^\sigma = I^\sigma(E) - I^\sigma$ is the light intensity change from I^σ (at $E = 0$) to $I^\sigma(E)$ in the presence of E and $OD^\sigma(E)$ and OD_0^σ are the optical densities at E and at $E = 0$, respectively.

The absorbance A^σ of the reporter lipid β-DPH pPC in the bilayer of the vesicles is given by the difference ΔOD^σ between $OD^\sigma(V, D)$ of the doped vesicles and $OD^\sigma(V)$ of the vesicle without the reporter lipid, but at the same total lipid concentration and vesicle size: $A^\sigma = OD^\sigma(V, D) - OD^\sigma(V)$. Therefore, the field induced change ΔA^σ in the absorbance of the β-DPH pPC doped vesicles is determined by

$$\Delta A^\sigma = \Delta(\Delta OD^\sigma) = \Delta OD^\sigma(V, D) - \Delta OD^\sigma(V) \quad (2)$$

For the analysis of the actually determined relative absorbance changes $\Delta A^\parallel$ and $\Delta A^\perp$ at the two light polarization modes $\sigma = 0°$ (parallel) and $\sigma = 90°$ (perpendicular), respectively, are referred to the zero-field absorbance A_0. The difference between $\Delta A^\parallel$ and $\Delta A^\perp$ is, to a good approximation, equal to the electric linear dichroism ΔA. The dichroism is a quantitative measure of the orientational changes of the optical transition moments of the DPH probes, and thus a measure of rotational changes of the probe molecules taken along with the lipid molecules. The reduced linear dichroism $\Delta A/A_0$ is given by (Kakorin and Neumann 1996):

$$\frac{\Delta A}{A_0} \approx \frac{\Delta A^-}{A_0} = \frac{(\Delta A^\parallel - \Delta A^\perp)}{A_0} \quad (3)$$

In addition to the DPH dichroism, the weighted sum ΔA_{CH} of the measured absorbance modes reflects changes in the immediate environment of the β-DPH pPC reporter lipid due to entrance of water and small ions into the lipid phase in the process of pore formation (Revzin and Neumann 1974):

$$\frac{\Delta A_{CH}}{A_0} = \frac{(\Delta A^\parallel + 2 \cdot \Delta A^\perp)}{3 A_0} \quad (4)$$

It is recalled that the electric field effect is indirect. The external field E causes interfacial polarization such that the actual membrane field is given by

$$E_m = -\Delta\varphi / d = 1.5 \cdot E \cdot (a/d) \cdot f(\lambda_m) \cdot |\cos\theta| \quad (5)$$

where $\Delta\varphi$ is the induced transmembrane electric potential difference across the membrane of thickness d at the opening angle θ of a polar coordinate system of a vesicle of radius a; $f(\lambda_m)$ is the conductivity factor and λ_m is the membrane conductivity (Neumann 1989).

III Results

The optical density spectrum $OD(\lambda)$ of the suspension of lipid vesicles is characteristically modified by the membrane probe β-DPH pPC (Fig. 1) owing to absorbance contributions of the chromophores to the turbidity of the pure vesicles, originating principally from vesicle light scattering. It was found that the absorbance contribution of the β-DPH pPC doped vesicles at the wavelength $\lambda = 365$ nm is very sensitive to structural and environmental changes in the lipid membrane (Kakorin et al. 1996). The optical

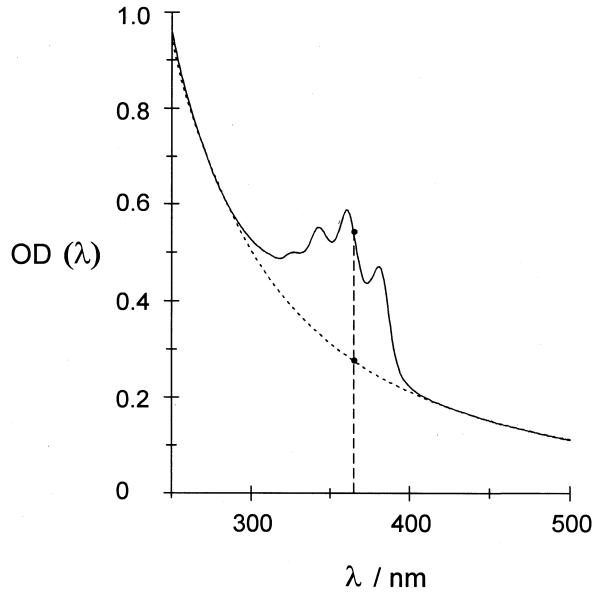

Fig. 1 Optical density (*OD*) of a suspension of unilamellar vesicles composed of L-α-phosphatidyl-L-serine (*PS*) and 1-palmitoyl-2-oleoyl-sn-glycero-3-phosphocholine (POPC) at a molar ratio PS: POPC of 1 : 2 (*dashed line* ---) and the same suspension doped with 2-(3-(diphenylhexatrienyl)propanoyl)-1-hexadecanoyl-sn-glycero-3-phosphocholine (β-DPH pPC, $M_r = 782$) (*solid line* —) as a function of the wavelength λ. Vesicle radius a = 90 nm, total lipid concentration $[L_T] = 1.0$ mM; [β-DPH pPC_T] = 5 μM; vesicle density $\rho_V = 2.1 \cdot 10^{15}\ L^{-1}$, buffer 0.66 mM HEPES-Na (pH = 7.4) containing 130 μM $CaCl_2$, T = 293 K (20 °C)

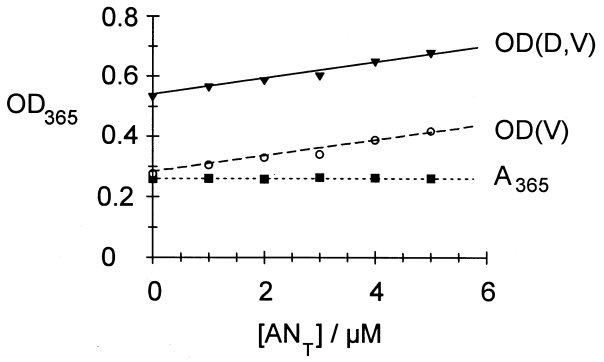

Fig. 2 Optical density OD_{365} (V) at $\lambda = 365$ nm of a vesicle suspension (○) and OD_{365} (D, V) of a β-DPH pPC-doped vesicle suspension (▼) at the same lipid concentration, as a function of the total annexin V concentration [AN_T]. The OD increases because of the Ca^{2+} mediated binding of annexin to the membrane. The absorbance (A_{365}, ■) of the "reporter lipid" β-DPH pPC (e.g. at $\lambda = 365$ nm) is given by $A_{365} = \Delta OD_{365} = OD_{365}$ (D, V) – OD_{365} (V) and is not measurably affected by the protein

transition moment of the chromophore DPH of β-DPH pPC apparently indicates changes caused by the entrance of water, ions or proteins. The local electric field of small ions approaching the vicinity of the optical membrane probe is very high and produces a so-called "iono-electrochromic" effect (Kakorin et al. 1996), leading to finite values of ΔA_{CH}. The progressive addition of annexin V (AN) increases the optical density of both pure and doped vesicles (Fig. 2). It is interesting that the OD-values increase in parallel with increasing [AN_T] such that the difference OD(V, D) – OD(V) of the optical densities of the pure (OD(V)) and doped vesicles (OD(V, D)), being the absorbance A of β-DPH pPC, remains constant, regardless of the annexin concentration in the region $0 \le [AN_T]/\mu M \le 5$. Obviously, the binding of AN to the outer surface of the vesicle membrane increases the light scattering properties of the vesicles, but does not effect the absorbance characteristics of the β-DPH pPC; note that the DPH part of the membrane probe is located deeper in the membrane, making apparently no optically visible contact with the protein.

However, in externally applied electric fields, the presence of AN dramatically changes the kinetics of both the chemical absorbance mode $\Delta A_{CH}/A_0$ (Fig. 3a) and the difference $\Delta A^-/A_0$ (Fig. 3b). Specifically, the time course of the chemical absorbance mode exhibits an extremum (Fig. 3a). Furthermore, in the entire external field strength

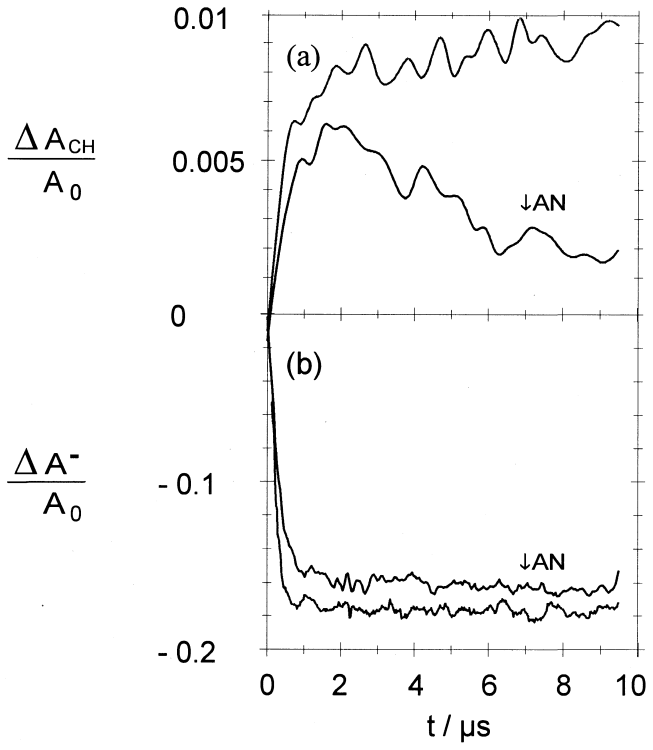

Fig. 3 **a** The chemical contribution $\Delta A_{CH}/A_0 = (\Delta A^{\parallel} + 2\Delta A^{\perp})/(3A_0)$ and **b** the difference $\Delta A^-/A_0 = (\Delta A^{\parallel} - \Delta A^{\perp})/A_0 \approx \Delta A/A_0$ (reduced dichroism) of the relative absorbance changes at the parallel ($\sigma = \parallel$) and perpendicular ($\sigma = \perp$) light polarization modes ($\lambda = 365$ nm), respectively, with and without annexin V (↓AN), as functions of time at the field strength E = 6.0 MV m^{-1}. Rectangular electric pulse duration $t_E = 10$ μs at T = 293 K (20 °C). The zero-field absorbance of β-DPH pPC is $A_0 = OD_0$ (V, D) – OD_0 (V) = 0.259 and $A_0 = 0.264$ in the presence of 4 μM annexin V, where OD_0 (V, D) and OD_0(V) are the measured optical densities OD_0 of the doped (V, D) and non-doped (V) vesicle suspension, respectively. Experimental conditions as in Fig. 1

region $2 \le E/MV\ m^{-1} \le 8$, the AN binding to the vesicle surface not only decreases the amplitudes of the chemical absorbance change $\Delta A_{CH}/A_0$ (Fig. 4a) and of $\Delta A^-/A_0$ (Fig. 4b), but also reduces the relaxation rate (τ^{-1}) of the optical signals (Fig. 4c). At constant annexin concentration [AN_T] and vesicle curvature H = 1/a, the relaxation rate τ^{-1} and the amplitudes of ΔA^- and ΔA_{CH} increase with increasing field strength E (Fig. 4). An interesting finding is that the vesicle curvature very strongly influences the field-induced absorbance changes (Fig. 5). For the following analysis, the curvature and the external field were chosen such that all data points in Fig. 5 refer to the same (constant) E_m value.

The relative decrease of the amplitudes of ΔA_{CH}, ΔA^- and the relaxation rate τ^{-1} with increasing annexin V concentration [AN_T] reflects a kind of inhibitory effect on ME by increasing amounts of bound annexin V.

We may specify the inhibitory effect of AN on ME by $\Delta(\Delta A) = \Delta A(0) - \Delta A([AN_T])$, where $\Delta A(0)$ refers to the field induced absorbance change at $[AN_T] = 0$ and $\Delta A([AN_T])$ to a given total AN concentration. Defining

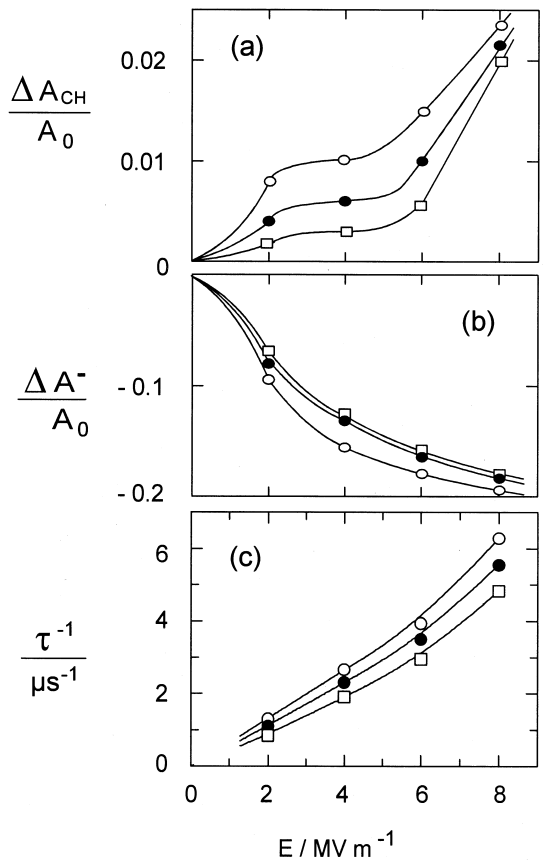

Fig. 4a–c The amplitudes of (**a**) the chemical term $\Delta A_{CH}/A_0$ and (**b**) the difference $\Delta A^-/A_0$ and (**c**) the normal mode relaxation rate τ^{-1} of the rapid phase, as functions of the electrical field strength E, at zero (○), 2 μM (●), and 4 μM (□) total concentrations of annexin V, respectively. Rectangular electric pulse of the field strength E and pulse duration t_E = 10 μs at T = 293 K (20 °C). Experimental conditions as in the Fig. 1

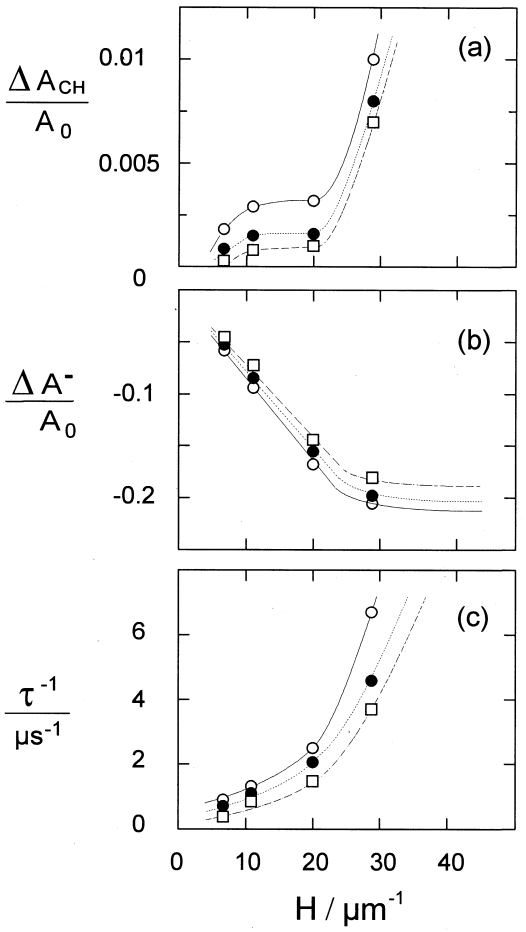

Fig. 5a–c The effect of vesicle size on the extent and rate of electroporation at zero (○), 2 μM (●), and 4 μM (□) total concentrations of annexin V, respectively. The amplitudes of (**a**) the chemical term $\Delta A_{CH}/A_0$, (**b**) the difference $\Delta A^-/A_0$ and (**c**) the normal mode relaxation rate τ^{-1} as functions of the vesicle curvature H = 1/a at constant total lipid concentration [L_t] = 1.0 mM and the same nominal transmembrane voltage drop $\Delta\varphi_m^N = -1.5 \cdot a \cdot E = -0.3$ V. Other experimental conditions as in Fig. 1 and Fig. 4. The fact that the values $|\Delta(\Delta A^-)/\Delta A(0)|$ and τ^{-1} are increasing with H is in line with the electroporation model, not with a simple elongation of the vesicle sphere to an ellipsoidal shape, at the expense of area reservoirs such as undulations

now a reduction factor by

$$f = |\Delta(\Delta A)/\Delta A(0)| \qquad (6)$$

we see in Fig. 6 that both the chemical reduction factor f_{CH} for ΔA_{CH} as well as the dichroitic reduction factor f_{OR} for ΔA^-, increase up to a saturation value at $[AN_T]_{sat} \approx 4$ μM at the given conditions of lipid concentration, vesicle radius, field strength and pulse duration. Similarly, the rate reduction factor $f_\tau = |\Delta\tau^{-1}|/\tau^{-1}(0)$ increases with [AN_T]. It is noted that the half saturation concentrations $[AN_T]_{hs} \approx 1.3$ μM are the same for all three reduction factors.

In the simplest case of a 1:1 binding stoichiometry between AN and membrane surface sites B according to $AN + B \rightleftharpoons AN_b$, where AN_b is bound (adsorbed) AN,

the equilibrium constant is $K_{AN} = [AN]\,[B]/[AN_b] = [AN]\,(1-\alpha)/\alpha$, where $\alpha = [AN_b]/[B_T]$ is the degree of AN binding and $[B_T]$ is the total concentration of binding sites. Mass conservation in terms of $[AN_T] = [AN] + [AN_b]$ yields

$$[AN_T] = K_{AN}\,\alpha/(1-\alpha) + \alpha[B_T] \quad (7)$$

At a lipid concentration of $[L_T] = 1.0$ mM, the outer leaflet lipid concentration is ≈0.5 mM. If one bound AN molecule covers 26 lipid head groups (Huber at al. 1992; Meers and Mealy 1993 b), the total concentration of potential binding sites for a (hypothetical) dense monolayer coverage is $[B_T] = 0.5$ mM/26 ≈ 20 μM. With Eq. (7) it is readily shown that with $K_{AN} \approx 10^{-4}$ μM (Schlaepfer et al. 1987; Tait et al. 1989; Tait and Gibson 1992) and $[B_T] \approx 20$ μM, α increases linearly with increasing $[AN_T]$ up to $\alpha \approx 1$. Therefore $[AN_b] \approx [AN_T]$ and at $[AN_T]_{sat} \approx 4$ μM the degree of membrane coverage is a ≈0.2. Hence at 20% membrane coverage the inhibitory effect of bound AN reflected in the optical data is saturated.

The results of the theoretical data analysis below suggest that the gradient in the lipid packing density across the membrane is responsible for both the curvature (Fig. 5) and the AN (Fig. 6) effects.

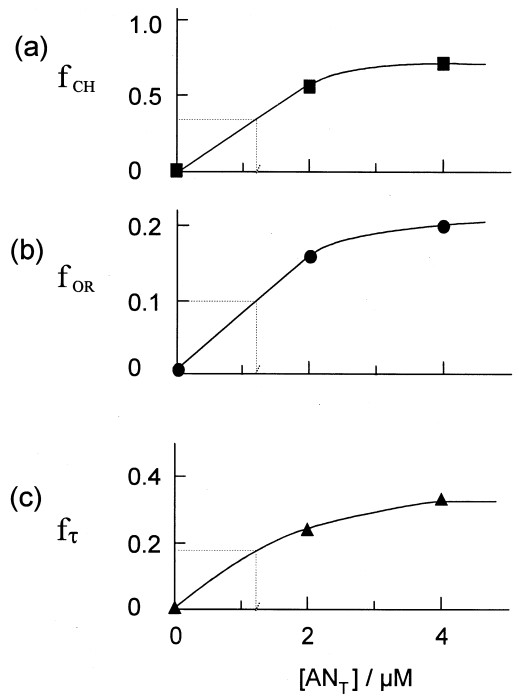

Fig. 6a–c The inhibitory effect of annexin V binding on the extent and rate of electroporation. (**a**) The chemical reduction factor $f_{CH} = |\Delta(\Delta A_{CH})/\Delta A_{CH}(0)| = |(\Delta A_{CH}(0) - \Delta A_{CH}([AN_T]))/\Delta A_{CH}(0)|$, (**b**) the dichroitic reduction factor $f_{OR} = |\Delta(\Delta A^-)/\Delta A(0)| = |\Delta A^-(0) - \Delta A^-([AN_T]))/\Delta A^-(0)|$, and (**c**) the reduction factor $f_\tau = |\Delta\tau^{-1}|/\tau^{-1}(0) = |\tau^{-1}(0) - \tau^{-1}([AN_T])|/\tau^{-1}(0)$ of the normal mode relaxation rates as functions of total annexin V concentration $[AN_T]$. The data refer to the field strength E = 4 MV m^{-1} and vesicles of a = 100 nm. Other experimental conditions as in Fig. 5. Note that the half saturation concentrations $[AN_T]_{hs} \approx 1.3$ μM of the inhibitory AN effect are the same for all three relaxation parameters

IV Theory and data analysis

Field induced elongation of the spherical vesicle to an ellipsoid can lead to a dichroitic optical signal ΔA^-. However, the vesicle deformation at constant membrane area requires a volume reduction, thus is very slow and should not lead to a finite value of ΔA_{CH} at a pulse duration of 10 μs (Neumann and Kakorin 1996). It turns out that the amplitude of the optical signal calculated for potential vesicle deformation with a non-electroporated membrane area is tenfold smaller than the actually observed values, if the vesicle membrane possesses a lateral tension of $\sigma \approx 10^{-3}$ N/m (Steiner and Adam 1984). In brief, the result of a lengthy theoretical analysis of the data is that the extent of the absorbance changes (Fig. 5) is due to global vesicle shape deformation rapidly coupled to the increase in the membrane area caused by the formation of aqueous electropores. The small membrane area increase (≤0.2% of the total membrane area (Hibino et al. 1993)) at constant vesicle volume results in a small vesicle elongation because of the electrical Maxwell stress acting predominantly in the vesicle equatorial region. The extent of the ellipsoidal elongation of the vesicle can be expressed by the axis ratio p. A change in p, relative to p = 1 (spherical vesicle) is caused by an increase in the membrane surface (and membrane volume) due to aqueous electropores; the relative change Δp/p usually does not exceed 0.1 (data not shown). Theoretical analysis demonstrates that such a small extent of vesicle elongation is sufficient to describe the absorbance dichroism (Kakorin and Neumann, unpublished data). Therefore, the electro-optical data are interpreted in terms of structural changes leading to pore states (P).

Reaction scheme for the pore formation

As previously shown, the electro-optical relaxation data of DPH molecules embedded in the lipid phase are satisfactorily described in terms of local lipid phase transitions involving cooperative clusters L_n of n lipids in the pore edge (Kakorin et al. 1996). The data were analyzed with the scheme:

$$C \underset{k_{-1}}{\overset{k_1}{\rightleftharpoons}} (P) \quad (8)$$

The state transition from the closed, non-porous bilayer state C to the pore states (P) turns out to be the origin and the rate limiting step for the rapid vesicle shape deformation (time constant $\tau_1 \leq 0.2$ μs). Obviously, $K = [(P)]/[C] = k_1/k_{-1}$ is the equilibrium constant of the electroporation step, i.e. the entrance of water and ions forming aqueous electropores; k_1 and k_{-1} are the rate coefficients of pore formation (k_1) and pore resealing (k_{-1}).

When AN is bound to the vesicle membrane, the electro-optical signals change. At higher field strengths, E ≥ 6.0 (±0.2) MV m^{-1}, and larger vesicle radii (a ≥ 100 nm), a slower second relaxation mode is apparent, in particular

for ΔA_{CH} ($\tau_{II} \approx 14\,\mu s$, Fig. 3a). The slower relaxation mode of ΔA_{CH} can be described with a reaction scheme analogous to the scheme (8), but with the different rate constants: k_1^{AN} and k_{-1}^{AN}. The slow mode is modeled by the reaction cascade $C^{AN} \rightleftharpoons (P)^{AN}$, following the rapid state sequence $C \rightleftharpoons (P)$. Therefore the additional slow reaction mode is considered as practically independent of the rest of the membrane, occurring very probably in the membrane patches of the 26 lipids covered by one annexin V molecule. The origin of the slow reaction sequence is thus attributed to the membrane electroporation of membrane sites which are in direct contact with annexin V. The second mode of the dichroitic term ΔA^- connected with the $(P)^{AN}$ pore production is so slow that only its onset is observable at 10 μs (Fig. 3b). The slow ΔA_{CH} relaxation mode, with opposite sign compared to the rapid ΔA_{CH} mode (Fig. 3a) shows that membrane electroporation apparently affects the environment of the lipid reporter molecule β-DPH pPC in the protein/lipid 'interface pore' differently from that of the electropores in the rest of the membrane.

In summary, annexin V changes the sensitivity to electroporation of both membrane surface regions, covered and non-covered by annexin V. If the sole effect of increasing AN binding is an increasing reduction of the membrane area available for ME, the relaxation rate of ME in the remaining membrane, not covered by AN should not change. Apparently the bound AN exerts a long-range allosteric effect on the rest of the membrane such that ME is slowed down by 37% at $[AN_T]_{sat}$ (Fig. 6c). Compared with 20% membrane coverage ($\alpha = 0.2$), 20% reduction in the dichroitic signal $\Delta A^-(f_{OR} = 0.2)$ and 70% decrease in ΔA_{CH} ($f_{CH} = 0.7$) suggest that the optical changes of the rapid mode arise predominantly from the major part of the membrane not covered by AN. Remarkably, the mechanism by which bound AN acts allosterically on ME in the rest of the membrane can be related to curvature effects.

Area-difference-elasticity energy concept

The curvature effects can be rationalized with the concept of *area-difference-elasticity* (ADE) Gibbs energy developed by Evans (1974), Wiese et al. (1992), Sackmann (1995), Seifert and Lipowsky (1995). The curvature of vesicle membrane means a different packing density of lipid molecules in the outer and in the inner leaflets of the bilayer, respectively, causing a gradient in the lateral pressure across the vesicle membrane (Fig. 7a). The electro-optical data suggest that the gradient in the lateral pressure across the vesicle membrane facilitates the formation of (conical) electropores (Fig. 7b). Insertion of a part of the annexin molecule, perhaps the aromatic residue of the tryptophan (W 187), in the outer membrane leaflet can increase the packing density and thus reduce the gradient. This, in turn, reduces relaxation rate and extent of the electroporation process.

The total ADE-Gibbs energy reflects the deviation of the area difference, ΔS, between the two monolayers, from

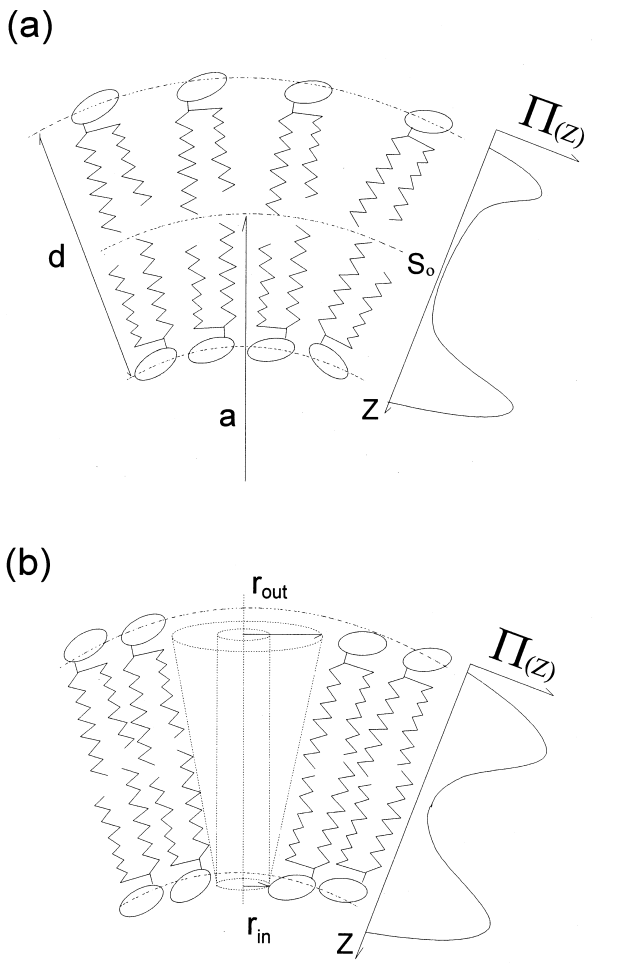

Fig. 7a, b Area-difference-elasticity (ADE) energy scheme. The area-difference-elasticity energy appears whenever the number of molecules within the two monolayers do not completely fill the membrane space. The vesicle membrane curvature is associated with a lipid packing difference between the two membrane leaflets and a lateral pressure gradient $d\Pi(z)/dz$ across the membrane (**a**). Membrane electroporation causing conical hydrophobic (HO) pores reduces the lipid packing density difference between the two monolayers and, consequently, the gradient of lateral pressure across the membrane (**b**)

the equilibrium value $\Delta S_0 = (N^{out} - N^{in})/\phi_0$, where N^{out} and N^{in} are the total number of lipid molecules in the outer and inner leaflets, respectively, ϕ_0 is the equilibrium surface density of the molecules in a monolayer of a flat membrane. If the possibly small alterations in the chemical potentials of lipids with changing membrane curvature are neglected (Sackmann 1995; Seifert and Lipowsky 1995), the ADE-Gibbs energy is here reformulated as:

$$G_{ADE} = \frac{2 \cdot \pi \cdot \alpha \cdot \kappa}{S_0 \cdot d^2} \cdot (\Delta S - \Delta S_0)^2 \qquad (9)$$

where d is the membrane thickness, κ is the bending rigidity and α is a material parameter. Note that Eq. (9) for G_{ADE} is the same as Eq. (8) of Seifert and Lipowsky (1995); however in Eq. (9), d refers to the bilayer.

In the case of the spherical vesicle, the total curvature can be reduced to $H = 1/a$, where a is the radius of the mid-surface of the bilayer of area S_0, and the total surface area difference between the two monolayers (Fig. 7a), ΔS, is given by $\Delta S = 2 S_0 \cdot H \cdot d$.

The formation of the hydrophobic (HO) pores is primary in the electroporation process (Glaser et al. 1988), and the hydrophilic pore states may be rapidly coupled to the (HO) states (Kakorin et al. 1996). Therefore, for simplicity in our further analysis of the electrooptical data, we equate (P) = (HO). In contrast to cylindrical water filled HO pores of volume $V = \pi r_p^2 d$, where r_p is the pore radius, conical HO pores (Fig. 7) in the vesicle membrane reduce the lipid packing density difference and thereby the ADE-Gibbs energy. Equation (9) with $\Delta S_0 \approx 0$ (i.e., $N^{out} - N^{in} \approx 0$) and $\Delta S = 2 S_0 \cdot H \cdot d$ indicates that the larger the vesicle curvature H, the larger is the Gibbs energy dissipated by the pore formation. Therefore, our membrane electroporation model combined with the ADE-energy concept is appropriate to describe the dependence of the electro-optic relaxation data on the vesicle size (Fig. 5). The smaller the vesicle size the larger the curvature, and the more effective becomes the ADE-free energy source facilitating membrane electroporation.

In order to cover the various thermodynamic, mechanical and electrical contributions to pore formation, the equilibrium constant K_1 of the rate limiting step $C \rightleftharpoons (HO)$, scheme (8), is written in the form $RT \cdot \ln K_1 = -\Delta_R G^{\ominus}$ or (Neumann and Kakorin 1996):

$$RT \cdot \ln K_1 = -\left(\Delta_R G^{\ominus} + \int_0^L \Delta_R \gamma \, dL + \int_0^{S_p} \Delta_R \Gamma \, dS + \int_0^H \Delta_R \beta \, dH - \int_0^{E_m} \Delta_R M \, dE_m \right) \quad (10)$$

where $\Delta_R = d/d\xi$ and ξ is the extent of reaction; the term $\Delta_R G^{\ominus} = \sum_{\alpha} \sum_{j} (\nu_j \cdot \mu_j^{\ominus})^{\alpha}$ is the conventional standard reaction Gibbs energy where ν_j^{α} is the stoichiometric coefficient and $\mu_j^{\ominus \alpha}$ the standard chemical potential of the molecule j in the phase α; $\Delta_R M$ is the reaction dipole moment; γ is the line tension (or pore edge energy density) and L is the edge length; Γ is the surface energy density and S_p is the pore surface area in the plane of the membrane; β is the curvature energy term. The $C \rightleftharpoons (HO)$ state transition is characterized by $\int_0^L \Delta_R \gamma \, dL = N_A \cdot \int_0^L (\gamma_{HO} - \gamma_C) \, dL = N_A \cdot \gamma \cdot 2\pi \cdot r_p$, where N_A is Avogadro's constant, $\gamma = \gamma_{HO}$ is the HO pore line tension; $L = 2\pi r_p$ is the circumference and r_p the radius of the HO-pore; note that for a closed membrane $\gamma_C = 0$. The surface tension term $\int_0^{S_p} \Delta_R \Gamma \, dS$ is usually assumed to be small for the vesicle membrane. At the present stage of the theoretical analysis this term is therefore not considered.

The curvature energy term $\int_0^H \Delta_R \beta \, dH$ is now expressed as the decrease in the ADE-Gibbs energy due to the formation of one mole of conical pores:

$$\int_0^H \Delta_R \beta \, dH = \frac{2 \cdot \pi \cdot \alpha \cdot \kappa \cdot N_A}{N_p \cdot d^2 \cdot S_0} \cdot \{(\Delta S - \Delta S_p - \Delta S_0)^2 - (\Delta S - \Delta S_0)^2\} \quad (11)$$

where N_p is the total number of pores in the vesicle system; $\Delta S_p = 4\pi \cdot N_p \cdot r_p^2 \cdot \zeta$ is the total area difference produced by N_p conical pores. The mean pore radius r_p of a conical HO pore is defined as $r_p = (r_{out} + r_{in})/2$, where r_{out} and r_{in} are the pore radii in the outer and inner leaflets of the bilayer, respectively (Fig. 7b). The factor ζ is given by $\zeta = (r_{out} - r_{in})/(r_{out} + r_{in})$. If for the mean pore radius $r_p = 0.35$ nm (see Kakorin et al. 1996), the HO pore edge contains 7 lipid molecules in the outer leaflet and 5 lipid molecules in the inner pore leaflet, we obtain $\zeta = 0.352$.

The total surface fraction of water filled electropores is usually very small, maximum 0.2% (Hibino et al. 1993). Hence, $\Delta S_p \ll \Delta S - \Delta S_0$, and Eq. (11) may be rewritten as:

$$\int_0^H \Delta_R \beta \, dH \approx \frac{16\pi^2 \cdot \alpha \cdot \kappa \cdot r_p^2 \cdot \zeta \cdot N_A}{d^2} \cdot \left(\frac{N_1^{out} - N_1^{in}}{4\pi \cdot \phi_0} \cdot H - 2 \cdot d \right) \cdot H \quad (12)$$

where N_1^{out} and N_1^{in} are the number of lipid molecules in the outer and inner leaflet of one vesicle, respectively. If N_1^{out} and N_1^{in} are only slightly different, $\Delta S \gg \Delta S_0$ and Eq. (12) reads:

$$\int_0^H \Delta_R \beta \, dH \approx -\frac{32\pi^2 \cdot \alpha \cdot \kappa \cdot r_p^2 \cdot \zeta \cdot N_A}{d} \cdot H \quad (13)$$

The electric polarization term at the opening angle θ relative to the field direction in the polar coordinate system of the vesicle is expressed as (Neumann 1989):

$$\int_0^{E_m} \Delta_R M \, dE_m = \frac{9 \cdot \pi \cdot \varepsilon_0 \cdot a^2 \cdot (\varepsilon_w - \varepsilon_L) \cdot r_p^2 \cdot N_A}{8 \cdot d} \cdot f^2(\lambda_m(\theta)) \cdot \cos^2\theta \cdot E^2 . \quad (14)$$

Here, we may assume that the mean pore radius r_p is approximately constant, independent of H and E. The minimum pore radius corresponds to a minimum number of the lipid molecules constituting the pore edges and to a minimum in the unfavorable hydrophobic interaction energy between the pore walls. As an increase in r_p is limited by the increasing transmembrane conductivity (Glaser et al. 1988), the pore edge length L can be considered as constant. Equation (10) may therefore contain only two dominant terms:

$$K_1 = K_1^0 \cdot \exp\left[-\left\{ \int_0^H \Delta_R \beta \, dH - \int_0^{E_m} \Delta_R M \, dE_m \right\} / RT \right] \quad (15)$$

where

$$K_1^0 = \exp\left(-\left\{ \Delta_R G^{\ominus} + \int_0^L \Delta_R \gamma \, dL \right\} / RT \right)$$

is the value at $E = 0$.

The analysis of the data presented in Fig. 4 and in Fig. 5 in terms of Eq. (15) yields the curvature and the polarization energy terms. Because the data indicate that the curvature and polarization energies are affected by the annexin V binding to the vesicles, we use the AN concentration dependence (Fig. 6) in order to specify the modes of the AN-membrane interaction. For this purpose we relate the values of H and E such that the (nominal) transmembrane potential $\Delta\varphi_m^N = -1.5 \cdot E \cdot a = -1.5 \cdot E/H$ is constant regardless of E and H; here we chose $\Delta\varphi_m^N = -0.3$ V. Note that the field-induced transmembrane potential drop is position dependent and given by: $\Delta\varphi_m = \Delta\varphi_m^N \cdot f(\lambda_m) \cdot |\cos\theta|$; see also Eq. (5).

At the transmembrane potential $\Delta\varphi_m^N = -0.3$ V the extent of the electroporation is small; hence the vesicle membrane is practically non-conductive ($\lambda_m = 0$) and $f(\lambda_m) \approx 1$ for all vesicle sizes (Kakorin et al. 1996). Therefore, the total surface fraction of electropores at a given value of $\Delta\varphi_m^N$ is constant irrespective of the size of the spherical unilamellar vesicles. Because the membrane thickness is much smaller than the vesicle radius ($d \ll a$), the total membrane area of vesicles S_0 is practically independent of vesicle size at constant total lipid concentration. Thus the total area difference ΔS depends solely on H. Using Eq. (13) and Eq. (14), Eq. (15) can be rewritten in the logarithmic form:

$$\ln(K_1) = A_H + B_H \cdot H \qquad (16)$$

where

$$A_H = \ln(K_1^0) - \int_0^{E_m} \Delta_R M \, dE_m/(RT),$$

$$B_H = 32\pi^2 \cdot \alpha \cdot \kappa \cdot r_p^2 \cdot \zeta \cdot N_A/(d \cdot RT).$$

The equilibrium constant K_1 can be calculated for the vesicle pole cap regions ($\theta \approx 0$) from the $\Delta A^-/A_0$ and $\Delta A_{CH}/A_0$ relaxations (Fig. 3) as described by Kakorin et al. (1996). The analysis of the linear part of the $K_1(H)$ relationship (Fig. 8a) in terms of Eq. (16) yields the curvature energy term $\int_0^H \Delta_R \beta \, dH/RT = B_H \cdot H$. At curvature $6.7 \le H/\mu m^{-1} \le 20$, the values of $B_H \cdot H$ range from 4.8 to 14.5, 4.6 to 13.9 and from 4.4 to 13.3 for the three annexin concentration terms $[AN_T]/\mu M = 0$, 2 and 4, respectively.

At $H \ge 20\ \mu m^{-1}$ a deviation from linearity is observed (Fig. 8a) and the function $\ln(K_1(H))$ approaches a saturation value. For larger curvatures the numbers of lipid molecules in the inner and outer lipid leaflets of the vesicle membrane are significantly different and the approximation $N_1^{out} \approx N_1^{in}$ does not hold; hence Eq. (13) cannot be used any more. The saturation is described by the more elaborate Eq. (12).

Theory predicts that K_1 is exponentially dependent on E^2 as long as $f(\lambda_m) \approx 1$. The polarization energy is calculated from the linear part of the function $K_1(E^2)$ (Fig. 8b). At the chosen nominal transmembrane potential $\Delta\varphi_m^N = -0.3$ V, the electropores are dominantly in the vesicle pole caps (Kakorin et al. 1996). Therefore, for $\theta \approx 0°$ and $\theta \approx 180°$ and Eq. (15) is rewritten as

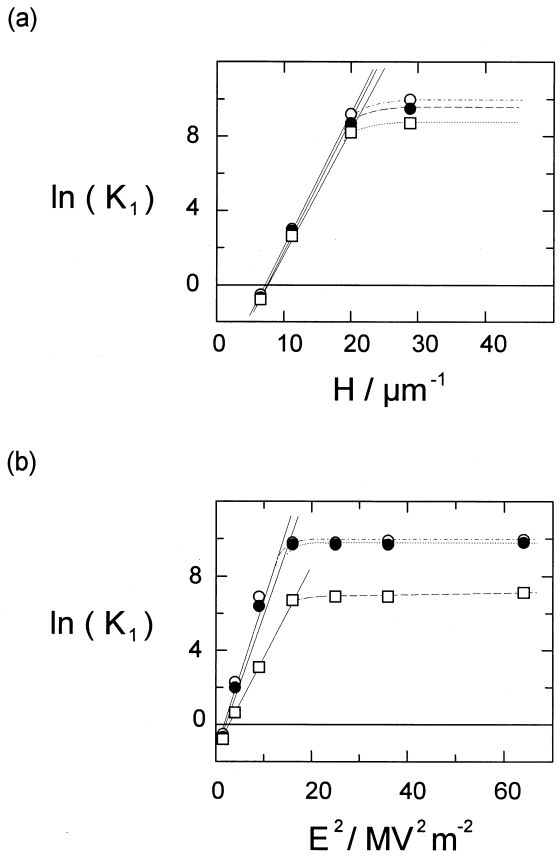

Fig. 8a, b The equilibrium constant K_1 (in terms of $\ln K_1$) of the electroporation state transition $C \rightleftharpoons HO$ from the closed membrane state (C) to the hydrophobic pores (HO) in the vesicle pole caps as a function (**a**) of the vesicle curvature H = 1/a at the nominal voltage $\Delta\varphi_m^N = -0.3$ V and (**b**) of the square of the external field strength for $H = 5\ \mu m^{-1}$ (a = 100 nm) at zero (○), 2 μM (●), and 4 μM (□) total concentrations of annexin V, respectively. The *solid lines* indicate the theoretically predicted linear courses, see Eq. (16) and Eq. (17) of the text. Experimental conditions as in Fig. 4 and Fig. 5

$$\ln(K_1) = A_E + B_E \cdot E^2 \qquad (17)$$

where $A_E = \ln(K_1^0) + B_H H$ and $B_E = 9 \cdot \pi \cdot \varepsilon_0 \cdot a^2 \cdot (\varepsilon_w - \varepsilon_L) \cdot r_p^2 \cdot N_A/(8 \cdot d \cdot RT)$.

At $H = 5\ \mu m^{-1}$ and in the field strength range $1 \le E/MVm^{-1} \le 4$, where Eq. (16) holds, the calculated polarization energy term $\int_0^{E_m} \Delta_R M \, dE_m/RT = B_E \cdot E^2$ ranges from 0.93 to 14.9, 0.87 to 13.9 and from 0.49 to 7.8 at annexin concentrations $[AN_T] = 0$, 2 and 4 μM, respectively.

Substitution of the polarization energy terms in Eq. (17) yields the pore radii $r_p/nm = 0.37$, 0.36, 0.27 at annexin concentrations $[AN_T] = 0$, 2 and 4 μM, respectively. Although the error margin of r_p is ±0.05 nm, the tendency of the radius to decrease with increasing annexin concentration is noticeable. The material parameter α is usually between 1 and 6 (Wiese et al. 1992; Seifert and Lipowsky 1995). For $\alpha = 3$ and d = 4 nm (Kummrow and Helfrich

1991), substitution of the values of r_p in the expression for B_H (Eq. (16)) yields the bending rigidity $\kappa/(10^{-19}\ \mathrm{J}) = 2.5$, 2.65 and 4.5 at annexin concentrations $[AN_T] = 0$, 2 and 4 μM, respectively. Although the error margin of κ is 10%, the apparent tendency of κ to increase with the increasing annexin concentration is clearly seen. Therefore, in terms of membrane bending rigidity, the bound annexin V interacts very strongly with the outer membrane leaflet and increases the bending rigidity of the whole membrane.

The 'zero field' equilibrium constant K_1^0 can be calculated either from Eq. (16) or from Eq. (17). Both equations yield practically the same value of $K_1^0 = (1.2 \pm 0.2) \cdot 10^{-2}$, in line with the concept of a characteristic mean pore radius, independent of the field. The numerical value of K_1^0 corresponds to a water content of ≈1.2% in the closed membrane state C at $E = 0$. The membrane water volume content of 9–21% in the head group region of egg-yolk phosphatidylcholine lipids in the liquid crystalline phase (McInosh and Magid 1993) suggests that in POPC vesicles there are probably only 0.5–1.0% water in the hydrocarbon region of the membrane. This estimate compares well with 1.2% derived from K_1^0.

If at a finite field strength the number of electropores in a vesicle and the factor ζ are unchanged by the adsorption of AN, a decrease in the equilibrium area difference ΔS_0 between the two leaflets causes a decrease in the mean pore radius. Assuming that the decrease in ΔS_p is approximately equal to the area occupied by the adsorbed AN in the outer membrane leaflet $\Delta S_{AN} \approx \Delta S_p(0) - \Delta S_p(AN)$, the relative area change due to partial intrusion of AN into the vesicle membrane is given by:

$$\frac{\Delta S_{AN}}{S_0} \approx \frac{r_p^2(0) - r_p^2(AN)}{r_p^2(0)} \cdot \frac{\Delta S_p(0)}{S_0} \qquad (18)$$

where $r_p(AN)$ and $r_p(0)$ are the pore radii in the presence and in the absence of annexin V, respectively.

If the maximum fraction of the porated membrane area is $\Delta S_p(0)/S_0 = 0.017\%$ (Kakorin et al. 1996), Eq. (18) yields the surface fraction of the outer leaflet occupied by annexin intrusions of $\Delta S_{AN}/\Delta S_0 \approx 0.01\%$ at $[AN_T] = 4$ μM. This is rather small, yet has a dramatic effect on the electroporatability.

V Discussion

It may be recalled that the 'zero field' light absorbance data (Fig. 2) showed that the binding of AN at $[Ca^{2+}] = 0.13$ mM, where all AN is completely bound, does not change the absorbance of β-DPH pPC in the vesicle membrane. Therefore AN adsorption alone does not cause water and ions to penetrate the vesicle membrane such that the deeper site of the DPH chromophore of β-DPH pPC is affected. It thus appears that AN does not produce conductive pores of the type described by scheme (8) in vesicle membranes in the absence of an external electrical field, i.e., in the absence of a transmembrane voltage. In contrast to the 'zero field' case, the second (slow) relaxation modes of ΔA_{CH} and ΔA^- (Fig. 3), becoming visible at $[AN_T] = 4$ μM and $E \geq 6$ MV m^{-1} in particular in the chemical contribution, are presumably due to electroporation of membrane patches which are in direct contact with the adsorbed protein. As the chemical term is responsible for the change of environment of the 'reporter lipids' (Kakorin and Neumann 1996), both the electric field and bound AN modify the membrane interior dramatically. Since the presence of solvated ions in the vicinity of β-DPH pPC in a pore edge causes an increase in the absorbance (positive ionochromic effect), the decrease in ΔA_{CH} of the second mode indicates the predominance of water entrance associated with the negative absorbance effect. The water entrance is probably caused by the delayed formation, or enlargement, of pores "under the protein", denoted as $(P)^{AN}$. The slow change in ΔA^- suggests a concomitant slow increase in $(P)^{AN}$-pore states. The second relaxation mode is consistent with the results of patch-clamp measurements (Burger et al. 1994), showing that annexin V produces ion selective channels under voltage clamp conditions.

The key for the identification of the annexin V/membrane interactions is the reduction of ΔA_{CH}, $|\Delta A^-|$ and τ^{-1} with increasing AN adsorption saturating at only 20% surface coverage by annexin V (Fig. 6). Obviously at $[AN_T] \geq 4$ μM, AN continues to bind to the vesicle membrane (Fig. 2). All the data suggest that the rapid relaxation mode refers to the remaining membrane, not covered by annexin V. Extent and rate of electroporation, increasingly reduced with increasing protein adsorption up to a saturation value, are quantitatively described in terms of curvature effects.

Alternatively to the vesicle curvature effect (Fig. 5), the reduction of ΔA_{CH}, $|\Delta A^-|$ and τ^{-1} with increasing $[AN_T]$ (Fig. 6) could be caused by 'annexin-made' electropores. Such additional pores would increase the transmembrane conductivity (λ_m) and thereby reduce the transmembrane field. However, as already discussed in the context of Fig. 2, the electro-optical relaxation data (Fig. 3), only indicate slow electropores associated with AN. The second mode of formation of electropores, probably in the membrane patches covered by AN, is more than ten times slower than that in the rest of the membrane. Thus a conductivity increase by 'annexin-made' electropores cannot describe the protein effect on the rapid mode of ME.

There is another possibility for the decrease in ΔA_{CH}, ΔA^- and τ^{-1} with increasing $[AN_T]$. The annexin-covered membrane patches have a larger thickness than the rest of the membrane. Therefore, at a given transmembrane voltage, the transmembrane field E_m (Eq. (5)) across the protein/membrane complex is smaller compared to the membrane and therefore both the extent and the rate of the electroporation process would be reduced. Again, the large changes in ΔA_{CH}, ΔA^- and τ^{-1} actually observed (Fig. 6) indicate that the (major) rapid relaxation mode reflects remote, allosteric changes in the electroporatability in the major part of the membrane not covered by AN. The local increase in the membrane thickness caused by AN adsorp-

tion can only rationalize the slow relaxation mode attributed to the sites of protein/membrane complexation.

In summary, the bound annexin V appears to act on the local curvature of the vesicle membrane. Both the decrease in the curvature energy term $\int_0^H \Delta_R \beta \, dH$ at constant $\Delta\varphi_m^N$ and the reduction of the pore radius r_p at constant curvature H with the increasing annexin concentration $[AN_T]$ suggest that AN partially penetrates the outer leaflet of the membrane. This partial penetration reduces the local curvature and thereby the gradient in the lateral pressure across the vesicle membrane. The fraction of membrane surface 'filled' by annexin is very small: ≈0.01% (Eq. (18)). Therefore, it is most likely that only a small molecular group, perhaps the aromatic part of the tryptophan residue, is inserted in the membrane. The saturation of the protein effect on ΔA_{CH}, ΔA^- and τ^{-1} (Fig. 6) indicates that at $[AN_T]_{sat}$ (≈4 μM) the lateral pressure gradient approaches zero as the annexin residue insertions in the outer membrane leaflet equalize the lipid packing densities between the two monolayer leaflets. As a consequence, these membrane patches become less curved or even planar. The ME data are thus also consistent with an AN induced vesicle shape transition (Andree et al. 1992) from a sphere to a 'polyeder', with bound AN positioned at the 'corners'.

References

Andree HAM, Stuart MCA, Hermens WTh, Reutelingsperger CPM, Hemker HC, Frederik PM, Willems GM (1992) Clustering of lipid-bound annexin V may explain its anticoagulant effect. J Biological Chemistry 267:17907–17912

Batchelor GK (1976) Brownian diffusion of particles with hydrodynamic interaction. J Fluid Mech 74:1–29

Brisson A, Mosser G (1991) Structure of soluble and membrane-bound human Annexin V. J Mol Biol 220:199–203

Burger A, Berendes R, Voges D, Huber R, Demange P (1993) A rapid and efficient purification method for recombinant annexin V for biophysical studies. FEBS 329:25–28

McIntosh ThJ, Magid AD (1993) Phospholipid hydration. In: Cevc G (ed) Phospholipids Handbook in Library of Congress Catalog-ing-in-Publication Data, New York, pp 553–578

Demange P, Voges D, Benz J, Liemann S, Göttig P, Berendes R, Burger A, Huber R (1994) Annexin V: the key to understanding ion selectivity and voltage regulation? TIBS 19:272–276

Evans E (1974) Bending resistance and chemically induced moments in membrane bilayers. Biophys J 14:923–931

Foster KR, Sowers AE (1995) Dielectrophoretic forces and potentials induced on pairs of cells in an electric field. Biophysical J 69:777–784

Funakoshi T, Heimark RL, Hendrickson LE, McMullen BA, Fujikawa K (1987) Human placental anticoagulant protein: isolation and characterization. Biochem 26:5572–5578

Glaser R, Leikin SL, Chernomordik LV, Pastushenko VF, Sokirko AI (1988) Reversible electrical breakdown of lipid bilayers: formation and evolution of pores. Biochim Biophys Acta 940: 275–287

Hibino M, Itoh H, Kinosita K Jr (1993) Time courses of cell electroporation as revealed by submicrosecond imaging of transmembrane potential. Biophys J 64:1789–1800

Heller R, Jaroszeski MJ, Glass LF, Messina JL, Rapaport DP, Deconti RC, Fenske NA, Gilbert RA, Mir LM, Reintgen DS: Phase I/II (1996) Trial for the treatment of cutaneous and subcutaneous tumors using electrochemotherapy. Cancer 77:964–971

Huber R, Römisch J, Paques E-P (1990a) The crystal and molecular structure of human annexin V, an anticoagulant protein that bind to calcium and membranes EMBO 9:3867–3874

Huber R, Schneider M, Mayr I, Römisch J, Paques E-P (1990b) The calcium binding sites in human annexin V by crystal structure analysis at 2.0 Å analysis. FEBS 275:15–21

Huber R, Berendes R, Burger A, Schneider M, Karshikov A, Luecke H (1992) Crystal and molecular structure of human annexin V after refinement. J Mol Biol 223:683–704

Kakorin S, Stoylov S, Neumann E (1996) Electro-optics of membrane electroporation in diphenylhexatriene-doped lipid bilayer vesicles. Biophys Chem 58:109–116

Kakorin S, Neumann E (1996) Chemical electro-optics and linear dichroism of polyelectrolytes and colloids. Ber Bunsenges Phys Chem 100:721–722

Kummrow M, Helfrich W (1991) Deformation of giant lipid vesicles by electric-fields. Phys Rev A 44:8356–8360

Liemann S, Benz J, Burger A, Voges D, Hofmann A, Huber R, Göttig P (1996) Structural and functional characterisation of the voltage sensor in the ion channel human annexin V. J Mol Biol 258:555–561

Mayer LD, Hope MJ, Cullis PR (1986) Vesicles of variable size produced by rapid extrusion procedure. Biophys Acta 885:161–168

Meers P (1990) Location of tryptophans in membrane bound annexins. Biochem 29:3325–3330

Meers P, Mealy T (1993a) Relationship between annexin V tryptophan exposure, calcium, and phospholipid binding. Biochem 32:5411–5418

Meers P, Mealy T (1993b) Calcium dependent annexin V binding to phospholipids: stoichiometry, specificity, and the role of negative charge. Biochem 32:11711–11721

Meers P, Mealy T (1994) Phospholipid determinants for annexin V binding sites and the role of tryptophan 187. Biochem 33:5829–5837

Mosser G, Ravanat C, Freyssinet J-M, Brisson A (1991) Sub-domain structure of lipid-bound annexin V resolved by electron image analysis. J Mol Biol 217:241–245

Neumann E (1989) The relaxation hysteresis of membrane electroporation. In: Neumann E, Sowers AE, Jordan C (eds) Electroporation and electrofusion in cell biology. Plenum, New York, pp 61–82

Neumann E, Schaefer-Ridder M, Wang Y, Hofschneider PH (1982) Gene transfer into mouse lyoma cells by electroporation in high electric fields. EMBO J 1:841–845

Neumann E (1992) Membrane electroporation and direct gene transfer. Bioelectrochem Bioenerg 28:247–267

Neumann E, Werner E, Sprafke A, Krüger K (1992) Electroporation phenomena – Electro-optics of plasmid DNA and of lipid bilayer vesicles. In: Jennings BR, Stoylov SP (eds) Colloid and molecular electro-optics. Bristol, UK: IOP Publ Ltd, pp 197–206

Neumann E, Kakorin S, Tsoneva I, Nikolova B, Tomov T (1996) Calcium-mediated DNA adsorption to yeast cells and kinetics of cell transformation. Biophys J 71:868–877

Neumann E, Kakorin S (1996): Electrooptics of membrane electroporation and vesicle shape deformation. Curr Opin Colloid Interface Sci 1:790–799

Ravanat C, Torbet J, Freyssinet J-M (1992) A neutron solution scattering study of annexin V and its binding to lipid vesicles. J Mol Biol 226:1271–1278

Raynal P, Pollard HB (1994) Annexins, the problem of assessing the biological role for a gene family of multifunctional calcium- and phospholipid-binding proteins. Biochim Biophys Acta 1197: 63–93

Revzin A, Neumann E (1974) Conformational changes in rRNA induced by electric impulses. Biophys Chem 2:144–150

Sackmann E (1995) Physical basis of self-organization and function of membranes: physics of vesicles. In: Lipowsky R, Sackmann E (eds) Structure and dynamics of membranes, 1A. Elsevier, North-Holland, pp 213–304

Schlaepfer DD, Mehlman T, Burgess WH, Haigler HT (1987) Structural and functional characterization of endonexin II, a calcium- and phospholipid-binding protein. Proc Natl Acad Sci USA 84: 6078–6082

Seifert U, Lipowsky R (1995) Morphology of vesicles. In: Lipowsky R, Sackmann E (eds) *Structure and dynamics of membranes*, 1A. Elsevier North-Holland, pp 403–463

Smith PK, Krohn RI, Hermanson GT, Mallia AK, Gartner FH, Provenzano MD, Fujimoto EK, Goeke NM, Olson BJ, Klenk DC (1985) Measurement of protein using bicinchoninic acid. Anal Biochem 150: 76–85

Steiner U, Adam G (1984) Interfacial properties of hydrophilic surfaces of phospholipid films as determined by method of contact angles. Cell Biophysics 6: 279–299

Swairjo MA, Roberts MF, Campos M-F, Dedman JR, Seaton BA (1994) Annexin V binding to the outer leaflet of small unilamellar vesicles leads to altered inner-leaflet properties: ^{31}P- and ^{1}H-NMR studies. Biochem 33: 10944–10950

Swairjo MA, Seaton BA (1994) Annexin structure and membrane interactions: a molecular perspective. Annu Rev Biophys Biomol Struct 23: 193–213

Tait JF, Gibson D, Fujikawa K (1989) Phospholipid binding properties of human placental anticoagulant protein-I, a member of the lipocortin family. J Biol Chem 264: 7944–7949

Tait JF, Gibson D (1992) Phospholipid binding of annexin V: effects of calcium and membrane phosphatidylserine content. Archives Biochem Biophys 298: 187–191

Voges D, Berendes R, Burger A, Demange P, Baumeister W, Huber R (1994) Three dimensional structure of membrane bound annexin V: a correlative electron microscopy X-ray crystallography study. J Mol Biol 238: 199–213

Voges D, Berendes R, Demange P, Benz J, Göttig P, Liemann S, Huber R, Burger A (1995) Structure and function of the ion channel model system annexin V. Adv Enzymol Relat Areas Mol Biol 71: 209–239

Wiese W, Harbich W, Helfrich W (1992) Budding of lipid bilayer vesicle and flat membranes. J Phys Condens Matter 4: 1647–1657

Winterhalter M, Helfrich W (1988) Deformation of spherical vesicles by electric fields. J Coll Interface Science 122: 583–586